APPENDIX C: Hydroclimatic reconstructions in the Lower Basin: Winter precipitation reconstruction of the Paria watershed

by Kiyomi Morino and David Meko,
Laboratory of Tree-Ring Research, The University of Arizona

Table of Contents

C.1 Introduction 2
C.2 Study Basin 2
C.3 Data 2
C.3.1 Precipitation Data 2
C.3.2 Tree-Ring Data. 2
C.4 Methods 3
C.4.1 Reconstruction Model 3
C.5 Results and Discussion 3
C.5.1 Reconstruction modeling 3
Tree-Ring Chronology Development 3
Single-Site Reconstruction 3
C.5.2 Reconstructed precipitation 4
C.6 Conclusions 4

TABLES 5
Table C-1. List of site chronologies. 5
Table C-2. Chronology basic statistics 6
Table C-3. Summary of single-site loess models 7
Table C-4. Summary of sub-period reconstruction models. 8

FIGURES 9
Figure C-1. Correlation of streamflow with seasonal precipitation. 9
Figure C-2. Monthly basin precipitation. 10
Figure C-3. Site map. 11
Figure C-4. PC loadings. 12
Figure C-5. Agreement of observed and reconstructed precipitation. 13
Figure C-6. Time plots of reconstructed winter precipitation 14

C.1 Introduction

Despite the long streamflow record (Paria at Lees Ferry; USGS ID: 09382000) and several high-quality tree-ring sites in and around the Paria River basin, initial efforts to develop a streamflow reconstruction were unsuccessful. Further analysis of the streamflow data offers a potential explanation. Early in the streamflow record, summer precipitation shows a high correlation with water year streamflow; indeed, it is higher than the correlation with winter precipitation (Figure C-1). By about 1960, the correlation between winter precipitation and streamflow increases to just under 0.8 and maintains this level of association for the duration of the streamflow record. Simultaneously, the association between summer precipitation and streamflow weakens until it hits a minimum of about 0.2 in the mid-1970s. In effect, the first half of the streamflow record was more strongly related to summer precipitation and was not tracked well by tree-ring indices. Exploratory comparisons between individual candidate sites and both water year and winter, October through April, precipitation indicated a slightly stronger association with winter precipitation. This hydroclimatic variable was subsequently targeted for reconstruction.

C.2 Study Basin

The Paria watershed (HUC: 14070007) is a small drainage of about 3,675 km^2 (908,000 acres) in size. Its headwaters are in the Pink Cliffs of Bryce Canyon National Park. At the Paria at Lees Ferry USGS gage, the mean daily discharge for water years over the period of record is 0.80 cms (28.1 cfs) (USGS 2012c). The highest water year mean was 1.84 cms (65.1 cfs) in 1980; the lowest was 0.31 cms (11.1 cfs) in 2002. Average water year runoff is 25.12 mcm (20.37 kaf).

C.3 Data

C.3.1 Precipitation Data

Precipitation data were derived from PRISM (Precipitation-elevation Regressions on Independent Slopes Model) data (Gibson et. al 2002). Monthly PRISM data, 1900-2010, for the continental US were downloaded from the PRISM site (http://prism.oregonstate.edu/products/). Data pertaining to the Paria watershed were "clipped" from the larger dataset using a script written in MatLab ™. Average precipitation depth in mm over the entire basin was computed. Precipitation is bi-modal with a larger winter and smaller summer contribution to annual precipitation (Figure C-2).

C.3.2 Tree-Ring Data.

Tree-ring data for this reconstruction consisted of measured ring-widths. These were obtained from the International Tree-Ring Data Bank (ITRDB) (http://www.ncdc.noaa.gov/paleo/treering.html) and from new sites collected not yet submitted to the ITRDB (Table C-1). The reconstruction developed in this study made use of 9 tree-ring chronologies. Sites were selected with the criteria that the species be moisture-sensitive and the data cover at least the period 1700-1964. The 1700 cutoff ensured that at least two centuries of reconstructed streamflow data could be later analyzed for patterns of temporal variability; the 1964 cutoff ensured a reasonably long period (64 years) for calibration of precipitation with tree rings in the reconstruction model.

See *Hydroclimatic Reconstructions in the Lower Basin of the Colorado River, METHODS* for details regarding tree-ring data standardization.

Following chronology development, both water year and winter, October through April, precipitation were compared to tree-ring data using simple correlation analysis. Winter precipitation showed a slightly stronger association with the tree-ring data and was targeted for reconstruction.

C.4 Methods

C.4.1 Reconstruction Model

See *Hydroclimatic Reconstructions in the Lower Basin of the Colorado River, METHODS* for details regarding methods employed in single-site reconstructions.

C.5 Results and Discussion

C.5.1 Reconstruction modeling

Tree-Ring Chronology Development

The set of 9 tree-ring chronologies passing the screening for sample depth and correlation with flow are listed in Table C-1. Their site locations are marked by shaded triangles on the map in Figure C-3. The common period is 1561-1998, though some extend to earlier and later years. Exploratory analysis pointed to 1550 as a feasible start year for reconstruction. All chronologies were therefore truncated to start in either 1550 or the first year with adequate subsample signal strength (SSS>0.85). Descriptive statistics showed that the chronologies have near-zero autocorrelation and negative skew (Table C-2). Skew is significantly (p<0.01) negative for all but one chronology. The near-zero autocorrelation is expected, as these are residual chronologies (Cook et al. 1990b).

Single-Site Reconstruction

The SSR models explain 25-51 percent of the variance of precipitation in the calibration period, which ranges in length from 98 to 110 years for the 9 sites (Table C-3). Calibration periods start with 1901 but end in different years (1998 to 2010) depending on either the collection date of the chronology or the last year of precipitation data, 2010. All models have some skill of verification, as indicated by an RE-statistic above zero.

The final selected smoothing parameter, α , for the SSR models ranges from 0.35 to 0.80. The variation in selected α reflects differences in curvature of the statistical relationship between precipitation and tree-ring index. Higher values indicate a more linear relationship.

Recalibration and Reconstruction

Summary statistics of the loess models used to recalibrate the scores of PC#1 of the SSRs into final estimates of winter precipitation are listed in Table C-4. The percentage of precipitation variance explained by the models ranges from 46 percent for Model A to 59 percent for Model B. All three models have positive skill, reflected by positive RE statistics for cross-validation, and the root-mean-square error increases only slightly (~5 percent) from the calibration to the

validation data. Figure C-4 shows the PC#1 loadings for each of the models. For Model B, Lower Henderson and Coal Bench show the highest loadings.

Uncertainty

The validation statistics mirror the calibration R^2 in supporting the superior accuracy of Model B over the other two models (Table C-4). Statistics for Model B are most relevant, as that model supplies most of the reconstructed precipitation values. The RMSE of cross-validation of Model B is 44.4 mm (1.7 in), which is about two-thirds the standard deviation of winter precipitation for the 1901-1998 calibration period of the model.

C.5.2 Reconstructed precipitation

Winter precipitation

Reconstructed winter precipitation, 1550 - 2010, is plotted in Figure C-6A along with a baseline at the long-term median of 180 mm (7.1 in) to facilitate identification of wet years and dry years. Reconstructed precipitation has a mean of 183 mm (7.2 in), is positively skewed (skew =0.10, p>0.05), not significantly autocorrelated (r_1=-0.014, p>0.05), and comparable to PRISM data, whose 1901-2010 mean is 186 mm (7.3 in).

The 1700s stand out as a period of prolonged high frequency of dry years (Figure C-6B). For most of the century, from half to two-thirds of the years in a sliding 30-yr window are below the long-term median. Prior to the 1700s, the driest period was the late 1500s. The frequency of dry years peaks in the late 1800s. The wettest period over the last 500 years was the early 1900s.

C.6 Conclusions

Apparent shifts over time in the importance of seasonal precipitation for streamflow of the Paria River precluded the development of a streamflow reconstruction. Winter precipitation, October through April, was identified as the alternative hydroclimatic variable to reconstruct. Regression models showed moderate to good skill in tracking basin-wide, winter precipitation. Up to 59 percent of the variance was explained with the tree-ring data. The reconstruction identified the 1700s as a dry period relative to the rest of the 500-plus year record. The wettest period was the early 1900s.

TABLES

Table C-1. List of site chronologies.

N[1]	Site[2]	Species[3]	Location[4] Lat	Lon	El(m)	Period[5]
1	Bryce Point	PSME	37.6	-112.2	2500	1312-1998
2	Upper Henderson	PSME	37.7	-111.9	3000	1259-2010
3	Yovimpa	PSME	37.5	-112.5	2750	1436-1998
4	Lower Henderson	PIED	37.6	-112.0	2100	1507-2010
5	Skutumpah Rd#2	PIED	37.5	-112.1	1900	1406-2000
6	Red Canyon	PIPO	37.4	-112.1	2134	1300-2011
7	Coal Bench	PIED	37.6	-112.0	2100	1555-2000
8	Round Valley	PIED	37.4	-111.9	2000	1561-1999
9	Allen Canyon	PIPO	37.7	-111.8	2164	1557-2011

1 Site number
2 Site name
3 Species code: PIPO is *Pinus ponderosa*; PIED is *Pinus edulis*; PSME is *Pseudotsuga menziesii.*
4 Latitude and longitude in decimal degrees, elevation in m above sea level
5 Start and end year of chronology, after trimming as described in text

Table C-2. Chronology basic statistics

						Replication and Common Signal[4]		
N	Length[1]	Mean	Stdev	Skew[2]	r(1)[3]	#Cores	SSS	EPS
1	449(169)	0.999	0.214	-0.44**	-0.04	5-21	0.87	0.83-0.95
2	461(166)	1.000	0.119	-0.56**	-0.08	19-50	0.97	0.95-0.98
3	449(154)	0.997	0.229	-0.46**	-0.05	11-30	0.95	0.91-0.97
4	419(189)	1.003	0.221	-0.48**	-0.07	3-28	0.86	0.83-0.98
5	367(151)	0.999	0.198	-0.47**	-0.07	3-18	0.88	0.83-0.96
6	433(233)	1.000	0.147	-0.84**	0.01	3-15	0.77	0.68-0.90
7	395(176)	0.998	0.230	-0.50**	-0.06	3-14	0.88	0.83-0.95
8	408(150)	1.000	0.212	-0.41**	-0.10	3-23	0.89	0.85-0.97
9	401(225)	1.002	0.186	-0.27*	0.07	4-12	0.90	0.84-0.94

1 Length of site chronology, with minimum segment length in parentheses
2 Skewness (*,** denote significance at 0.05, 0.01 level)
3 First-order autocorrelation (*,** denote r(1) significantly different from zero at 0.05, 0.01 level)
4 Range in number of cores, minimum value of subsample signal strength, and range in expressed population signal

Table C-3. Summary of single-site loess models.

	Calibration[2]			Validation[3]		
N[1]	Period	α	V	RMSE	RE	RMSE	Group[4]
1	1901-1998	0.60	0.37	52.1	0.34	54.0	AB
2	1901-2010	0.65	0.31	57.2	0.27	59.4	ABC
3	1901-1998	0.30	0.38	51.7	0.32	54.7	AB
4	1901-2010	0.40	0.51	48.4	0.47	50.6	BC
5	1901-2000	0.35	0.48	47.1	0.43	50.2	B
6	1901-2010	0.80	0.25	59.8	0.22	61.4	BC
7	1901-2000	0.30	0.48	47.3	0.41	50.8	B
8	1901-1999	0.40	0.46	48.2	0.41	50.8	B
9	1901-2010	0.60	0.41	53.0	0.38	54.9	BC

1 Site number, as in Table 1
2 Calibration statistics: N=period for estimation of loess curve,
 α=loess smoothing parameter,V=variance-explained decimal fraction,
 RMSE=root-mean-square error of calibration
3 Validation statistics from leave-1-out cross-validation:
 RE=reduction of error statistic, RMSE=root-mean-square error
4 Subperiod reconstruction groups, see Table 4

Table C-4. Summary of sub-period reconstruction models.

			Calibration[4]			Validation[5]	
N[1]	Period[2]	p[3]	α	V	RMSE	RE	RMSE
A	1550-1998	3	0.35	0.46	48.6	0.40	51.7
B	1634-1998	9	0.40	0.59	42.1	0.56	44.4
C	1611-2010	4	0.30	0.52	47.6	0.47	50.5

1 Sub-period model name
2 Starting and ending years of sub-period
3 Number of chronologies
4 Calibration statistics: α=loess smoothing parameter, V=variance-explained decimal fraction, RMSE=root-mean-square error of calibration
5 Validation statistics from leave-1-out cross-validation: RE=reduction of error statistic, RMSE=root-mean-square error

FIGURES

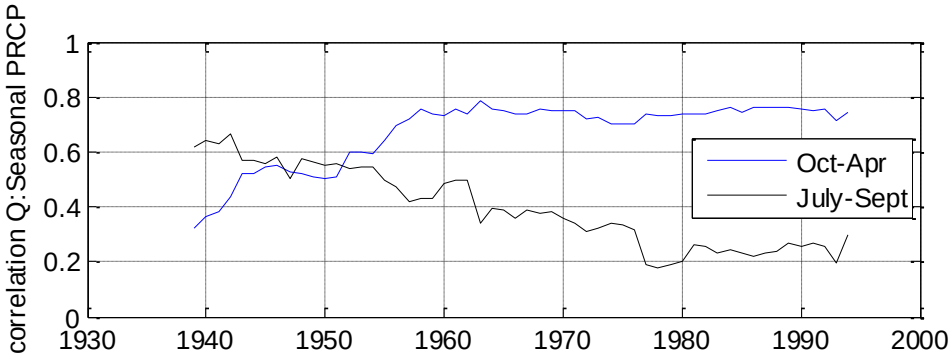

Figure C-1. Correlation of streamflow with seasonal precipitation.

Running 30-yr correlation between cool season (October – April) and warm season (July – September) precipitation and water year streamflow. At the beginning of the record, warm season precipitation shows a stronger relationship with streamflow; the opposite is true at the end of the record. Precipitation data is from PRISM; streamflow data is from Paria at Lees Ferry USGS gage (USGS ID: 09382000).

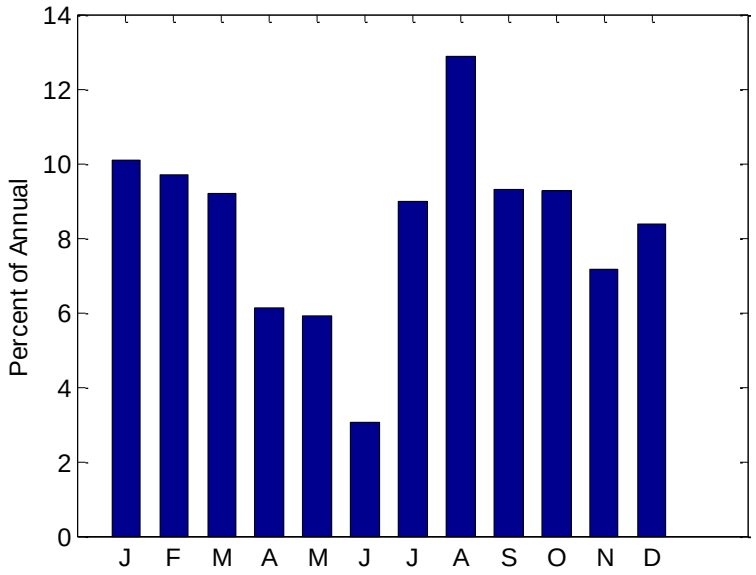

Figure C-2. Monthly basin precipitation.

Bar charts summarizing annual distribution of monthly basin precipitation, 1900-2010. Data from PRISM.

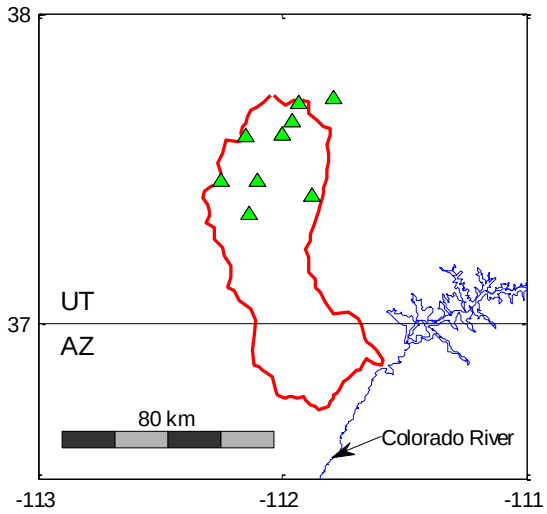

Figure C-3. Site map.

Map showing Paria watershed and tree-ring site locations. Tree-ring sites that passed screenings for sample depth and correlation with precipitation are denoted by green triangles.

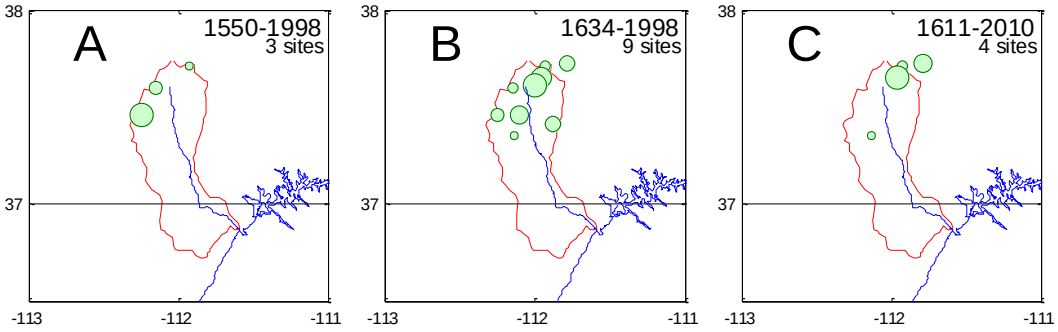

Figure C-4. PC loadings.

Tree-ring site locations for sub-period reconstruction models. Models A, B and C coded as in Tables 4. Symbol sizes reflect magnitude of loadings of sites on PC#1 of SSRs.

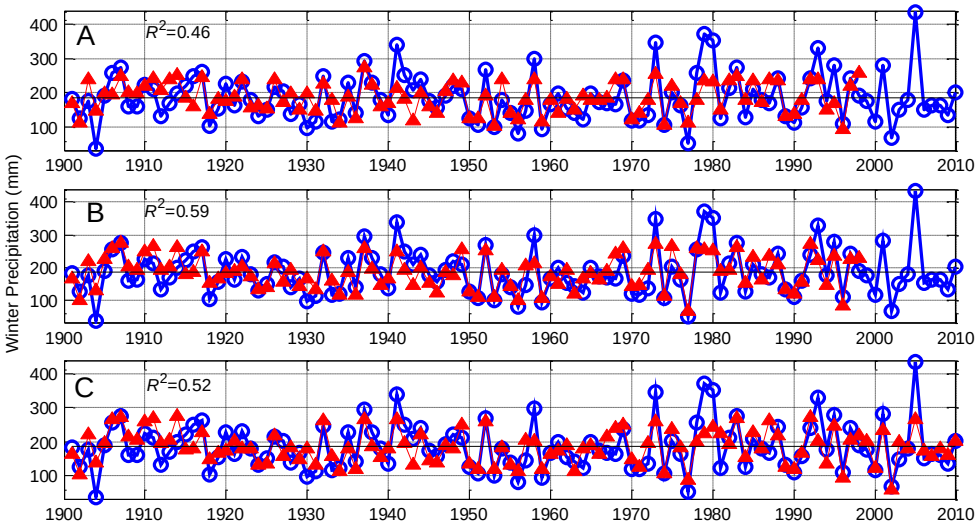

Figure C-5. Agreement of observed and reconstructed precipitation.

Agreement of observed and reconstructed precipitation for three sub-period models (as coded in Table 4). Annotated at upper left is the variance explained by the model. Horizontal line is the observed mean precipitation for the period, 1900-2010.

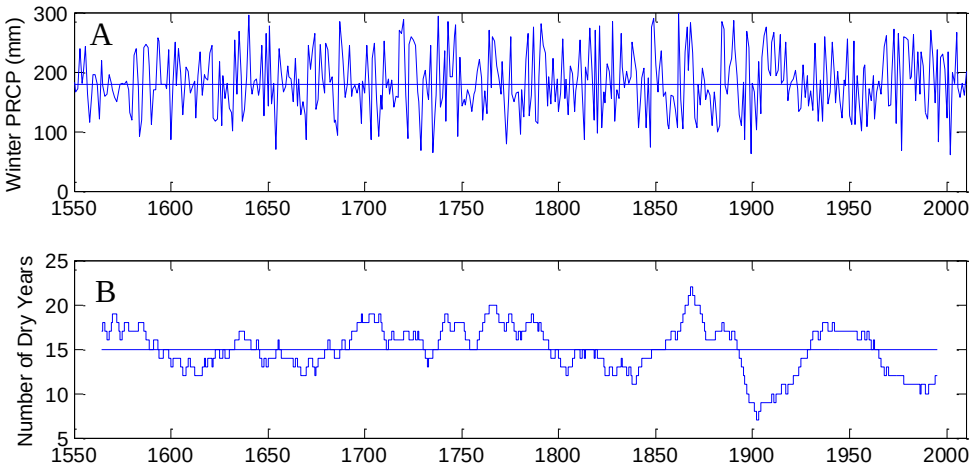

Figure C-6. Time plots of reconstructed winter precipitation.

Time plots of reconstructed years and dry-year frequency. (A) Reconstructed flows, 1496-2010, and dry year threshold (horizontal line) at median. (B) Frequency of dry years in centered 30-year moving window. Horizontal line in (B) is expected number of dry years in 30-year window.